Paper C

Higher Order Gradients on Unstructured Meshes Using Compact Formulation for Node-Centered Schemes

M. Carlsson, L. Davidson, S.H. Peng, and S. Arvidson. "Higher Order Gradients on Unstructured Meshes Using Compact Formulation for Node-Centered Schemes". ***2022 AIAA Aviation Forum.*** **June 2022.** DOI: 10.2514/6.2022-4156

Higher Order Gradients on Unstructured Meshes using Compact Formulation for Node-Centered Schemes

Magnus Carlsson *[1], Lars Davidson †[1], Shia-Hui Peng ‡ §[1,2], and Sebastian Arvidson ¶ ‖[1,3]
[1]*Chalmers University of Technology, SE-412 96, Gothenburg, SWEDEN*
[2]*Swedish Defence Research Agency, FOI, SE-16490 Stockholm, SWEDEN*
[3]*Saab Aeronautics, SE-581 88, Linköping, SWEDEN*

This paper introduces a new approach for gradient computations on node-centered unstructured grids. The proposed approach is to derive a gradient algorithm from a least squares approximation, where a local system is solved to introduce connectivity between neighbouring nodes. The resulting scheme forms a globally coupled linear system of equations for the gradients which can be solved efficiently by iterative techniques. Fourth-order gradient accuracy for interior nodes can be obtained on isotropic quadrilateral and mixed elements (quadrilaterals and triangles) grids. The same accuracy is achieved on quadrilateral and mixed elements grids with high-aspect-ratio. Additionally, a different formulation to the standard distance weighted least squares node-centered gradients is proposed, which shows robust second-order accuracy on grids with high-aspect-ratio compared to the standard formulation. The paper concludes with a proposed continuation for future developments.

I. Introduction

Computational Fluid Dynamics (CFD) tools are now routinely used for direct support/guidance of fast-paced engineering design processes in the aerodynamic industry. The gradient reconstruction scheme is a crucial part in a CFD analysis, which is closely associated to computational accuracy and efficiency, where the finite-volume methods is an industry standard. Finite volume discretizations are usually divided into cell-centered and node-centered approaches [1, 2]. In the cell-centered approach, the solution is defined at the centers of the grid elements, where the cell center coordinates are typically defined as the averages of the coordinates of the cell's vertexes. In the node-centered approach, the solutions are defined at the grid nodes. Control volumes are constructed around the grid nodes by a dual-grid, where the faces between control volumes are located at the midpoints between nodes. Since this study is focused towards a Node-centered finite-volume solver [3, 4], the focus is placed on a node-centered gradient reconstruction scheme.

Two common gradient reconstruction methods for unstructured finite-volume schemes are the Green-Gauss (GG) (see for example [5]) and Least Squares (LSQ) methods (see for example [6]). The LSQ method is a very popular method for unstructured grids, where the gradients are computed as a solution to a LSQ problem of fitting a polynomial over solution values in nearby cells. The LSQ method is more flexible than the GG method in that it is designed to be exact for linear functions on any type of grid, and also can be extended to high-order by fitting high-order polynomials. A drawback is, however, that high-order LSQ methods require large stencils, thus being less attractive for parallel implementation and for the construction of effective implicit solvers.

A recent approach called the variational reconstruction (VR) [7] method was proposed. In this method, a globally coupled system of linear equations for the gradients is found by minimizing the solution jumps at cell faces. The system is iteratively solved along with a finite-volume solver. In case that only one iteration is performed for the gradients per solver iteration, the cost per iteration is almost the same as the explicit methods suchs as the GG or LSQ methods. A similar approach, the Implicit Green-Gauss (IGG) gradient method [8], was derived from a second-order finite-volume discretization of a hyperbolic diffusion model. A common feature shared among these methods is that higher order can be achieved while still retaining a compact formulation. However, both methods were designed for cell-centered schemes, where the high accuracy gradients are assumed to be stored at the cell centers. Inspired by the these methods, we have explored a similar implicit gradient methodology, but targeted towards a node-centered scheme.

*PhD. student, Division of Fluid Dynamics, Department of Mechanics and Maritime Sciences, Chalmers University of Technology.
†Professor, Division of Fluid Dynamics, Department of Mechanics and Maritime Sciences, Chalmers University of Technology.
‡Guest Professor, Division of Fluid Dynamics, Department of Mechanics and Maritime Sciences, Chalmers University of Technology.
§Research Director, Division of Defense Technology, FOI. peng@foi.se, AIAA associate fellow.
¶PhD. Senior Engineer, Propulsion Aerodynamics and Performance, Saab Aeronautics
‖PhD. Visiting Researcher, Division of Fluid Dynamics, Department of Mechanics and Maritime Sciences, Chalmers University of Technology.

The presented work shares many similarities with high-order implicit finite difference (FD) methods called compact difference (CD) methods, also known as Padé schemes [9, 10]. The main difference between the CD and classical FD schemes is the computational stencil employed in the formulation of the discretization formulas. In the CD methods, the derivatives approximations are the results of solving linear systems of equations formulated based on coefficients calculated for all grid points along particular node lines. It makes the CD schemes much more accurate than FD methods. The CD schemes have been successfully applied on non-uniform meshes and in irregular domains, e.g. see [11–16]. However, in these works, the CD schemes are implemented with an underlying structure (Cartesian or curvilinear coordinate system) assumed. In the present work, we seek to extend the CD framework to fully unstructured grids, containing quadrilaterals, triangles or mixed elements.

The paper starts with the mathematical formulation of the implicit gradient scheme. A detailed investigation of the performance of the scheme to reproduce a known function on unstructured grids is then presented. Finally, some conclusions are made with a proposed continuation of the work.

II. Compact Gradient Reconstruction

A compact finite difference Padé scheme for approximating a derivative on a 1D grid can be written [9, 10, 17] as

$$\beta_{i+1}\left(\frac{\partial\phi}{\partial x}\right)_{i+1} + \beta_i\left(\frac{\partial\phi}{\partial x}\right)_i + \beta_{i-1}\left(\frac{\partial\phi}{\partial x}\right)_{i-1} = \gamma_{i+1}\phi_{i+1} + \gamma_i\phi_i + \gamma_{i-1}\phi_{i-1}, \tag{1}$$

where the coefficients $\{\beta_{i-1}, \beta_i, \beta_{i+1}, \gamma_{i+1}, \gamma_i, \gamma_{i-1}\}$ will set the order of the scheme. To obtain an approximation for the first derivative at node i, a polynomial can be fitted to pass through nodes $i-1, i, i+1$, where both the variable values at nodes $i-1, i, i+1$ and the first derivatives at nodes $i-1, i+1$ will be used. Using this compact formulation as in Eq. (1), a polynomial of fourth-degree can be constructed. Note that for a non-equidistant grid spacing, the coefficients in Eq. (1) need to depend on grid metrics to maintain a high order. The gradient scheme in Eq. (1) can be written as

$$P_{1D}\frac{\partial\boldsymbol{\phi}}{\partial x} = Q_{1D}\boldsymbol{\phi}, \tag{2}$$

which has to be solved each iteration if not the inverse solution $\frac{\partial\boldsymbol{\phi}}{\partial x} = P_{1D}^{-1}Q_{1D}\boldsymbol{\phi}$ can be easily found. To extend the compact scheme for higher dimensions, Eq. (1) can readily be applied along grid lines if the grid is structured (see e.g. Visbal et al. [11] for application in a curvilinear coordinate system). However, for an unstructured grid containing mixed elements (quadrilaterals and triangles) considered in this work, Eq. (1) can not be applied in a straight forward manner. In this work, we seek to derive an expression similar to Eq. (1) which is valid for higher dimensions on unstructured grids.

The derivation is made in 2D, the extension to 3D is straight forward. Consider a node i with a nearest neighbouring node j separated by a distance vector $\mathbf{d}_{ij}$, as shown in Fig. 1. Here, an unstructured grid containing mixed elements of quadrilaterals and triangles is considered, where only nodes j sharing an element with node i are included to maintain the compact formulation. The nodal value and the gradients of an arbitrary function ϕ at node j can be expressed from a polynomial expansion around node i:

$$\begin{aligned}
\phi_j &= \phi_i + \sum_{l=1}^{K}\sum_{m=0}^{l} a_k \Delta x_{ij}^{l-m}\Delta y_{ij}^{m}, \\
\left(\frac{\partial\phi}{\partial x}\right)_j &= \frac{1}{L_{i,x}}\sum_{l=1}^{K}\sum_{m=0}^{l} a_k (l-m)\Delta x_{ij}^{l-m-1}\Delta y_{ij}^{m}, \\
\left(\frac{\partial\phi}{\partial y}\right)_j &= \frac{1}{L_{i,y}}\sum_{l=1}^{K}\sum_{m=0}^{l} a_k \Delta x_{ij}^{l-m} m \Delta y_{ij}^{m-1}
\end{aligned} \tag{3}$$

where a_k is the unknown coefficients of the polynomial, $k = \frac{l(l+1)}{2} + m$ and K is the polynomial order. M is the number of terms in the polynomial expansion, where the relation between M and K is $M = \frac{K(K+3)}{2}$ in 2D. The normalized distances are expressed as

$$\Delta x_{ij} = \frac{x_j - x_i}{L_{i,x}}, \quad \Delta y_{ij} = \frac{y_j - y_i}{L_{i,y}} \tag{4}$$

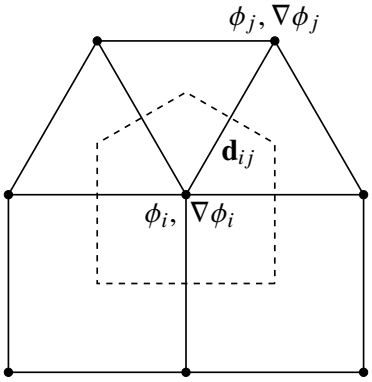

Fig. 1 Notation for dual grid control-volumes for a finite-volume discretization. The dual grid is generated from a node-centered unstructured grid.

where $L_{i,x}, L_{i,y}$ are normalization factors for node i. The choice of these factors are crucial to avoid growth of the condition number of the reconstruction matrix with grid refinement [18]. A natural choice is to choose the normalization according to the maximum distance to a neighbouring node j

$$L_{i,x} = L_{i,y} = \max_j d_{ij} \tag{5}$$

where

$$d_{ij} = |\mathbf{d}_{ij}| = \sqrt{(x_j - x_i)^2 + (y_j - y_i)^2} \tag{6}$$

is the distance between node i and neighbouring node j. In the work by Lou et al. [18] they tested a different normalization according to:

$$L_{i,x} = (x_{max} - x_{min})/2, \;\; L_{i,y} = (y_{max} - y_{min})/2, \tag{7}$$

which uses the local grid spacing in each coordinate direction. Here, $x_{max}, y_{max}, x_{min}$ and y_{min} are the maximum and minimum coordinates of node i and neighbouring nodes j in $x-$ and $y-$direction, respectively. This is helpful and important to remove the stiffness of the system matrices (Eqs. (9) and (13)) for higher-order approximations [18]. In this work, we also investigate a slightly different formulation, which can be seen as a combination of Eqs. (5) and (7), and is given by

$$L_{i,x} = \max_j |x_j - x_i|, \;\; L_{i,y} = \max_j |y_j - y_i|. \tag{8}$$

The coefficients a_k in Eq. (3) are estimated by summing over $j \in \{1, ..., N_b\}$ nearest neighbours to node i. This leads to the following set of equations:

$$\begin{bmatrix} \Delta x_{i1} & \Delta y_{i1} & \Delta x_{i1}^2 & \Delta x_{i1}\Delta y_{i1} & \Delta y_{i1}^2 & \cdots \\ \vdots & \vdots & \vdots & \vdots & \vdots & \ddots \\ \Delta x_{iN_b} & \Delta y_{iN_b} & \Delta x_{iN_b}^2 & \Delta x_{iN_b}\Delta y_{iN_b} & \Delta y_{iN_b}^2 & \cdots \\ 1 & 0 & 2\Delta x_{i1} & \Delta y_{i1} & 0 & \cdots \\ \vdots & \vdots & \vdots & \vdots & \vdots & \ddots \\ 1 & 0 & 2\Delta x_{iN_b} & \Delta y_{iN_b} & 0 & \cdots \\ 0 & 1 & 0 & \Delta x_{i1} & 2\Delta y_{i1} & \cdots \\ \vdots & \vdots & \vdots & \vdots & \vdots & \ddots \\ 0 & 1 & 0 & \Delta x_{iN_b} & 2\Delta y_{iN_b} & \cdots \end{bmatrix} \begin{bmatrix} a_1 \\ a_2 \\ a_3 \\ a_4 \\ a_5 \\ \vdots \\ a_M \end{bmatrix} = \begin{bmatrix} \phi_i(\mathbf{x_i}) - \phi(\mathbf{x_1}) \\ \vdots \\ \phi_i(\mathbf{x_i}) - \phi(\mathbf{x_{N_b}}) \\ L_{i,x}\frac{\partial \phi}{\partial x}(\mathbf{x_1}) \\ \vdots \\ L_{i,x}\frac{\partial \phi}{\partial x}(\mathbf{x_{N_b}}) \\ L_{i,y}\frac{\partial \phi}{\partial y}(\mathbf{x_1}) \\ \vdots \\ L_{i,y}\frac{\partial \phi}{\partial y}(\mathbf{x_{N_b}}) \end{bmatrix} \tag{9}$$

where $a_1 = L_{i,x}\frac{\partial \phi}{\partial x}(\mathbf{x_i})$ and $a_2 = L_{i,y}\frac{\partial \phi}{\partial y}(\mathbf{x_i})$ by construction. Equation (9) can be expressed as $Ax = b$, where A has the size $3N_b \times M$, x has the size $M \times 1$ and b has the size $3N_b \times 1$. The solution to Eq. (9) is found in a least squares sense, since the local system may be overdetermined, upon the number of neighbours N_b to node i and the polynomial order K assumed. Note that for a quadrilateral grid where each interior node has 8 neighbours sharing an element, we have $3N_b > M$ for a fourth-order polynomial.

The least square solution for Eq. (9) is found by minimising $||Ax - b||_2^2$, where the matrix A is decomposed using QR factorization via the Householder transformation [19]:

$$A = QR; \;\; Q^{-1} = Q^T; \;\; C = (A)^{-1} = R^{-1}Q^T, \tag{10a}$$

$$\Rightarrow x = Cb, \tag{10b}$$

where Q is an orthonormal matrix and R is an upper triangular, non singular matrix. Since we are only interested in the gradients, only the first two rows of C are kept. The higher order terms contribute to an increased accuracy of the gradients. The first two rows of C now contains the connectivity coefficients between the gradient at node i, nodal values at neighbouring nodes j and gradients at neighbouring nodes j. This can be seen from the the first two rows of Eq. (10b):

$$\begin{bmatrix} L_{i,x}\frac{\partial \phi}{\partial x}(\mathbf{x_i}) \\ L_{i,y}\frac{\partial \phi}{\partial y}(\mathbf{x_i}) \end{bmatrix} = \begin{bmatrix} C_{1j}b_j \\ C_{2j}b_j \end{bmatrix} \tag{11}$$

By expanding the terms on the right hand side of Eq. (11) and moving the terms which contains coefficients from neighbouring gradient values at nodes j to node i to the left hand side, we get the following linear system for node i:

$$\begin{aligned} L_{i,x}\left[\left(\frac{\partial \phi}{\partial x}\right)_i - \sum_{j=N_b+1}^{2N_b} C_{1j}^i \left(\frac{\partial \phi}{\partial x}\right)_j\right] - L_{i,y}\left[\sum_{j=2N_b+1}^{3N_b} C_{1j}^i \left(\frac{\partial \phi}{\partial y}\right)_j\right] &= \sum_{j=1}^{N_b} C_{1j}^i \phi_j - \phi_i \sum_{j=1}^{N_b} C_{1j}^i \\ L_{i,y}\left[\left(\frac{\partial \phi}{\partial y}\right)_i - \sum_{j=2N_b+1}^{3N_b} C_{2j}^i \left(\frac{\partial \phi}{\partial y}\right)_j\right] - L_{i,x}\left[\sum_{j=N_b+1}^{2N_b} C_{2j}^i \left(\frac{\partial \phi}{\partial x}\right)_j\right] &= \sum_{j=1}^{N_b} C_{2j}^i \phi_j - \phi_i \sum_{j=1}^{N_b} C_{2j}^i \end{aligned} \tag{12}$$

Equation (12) is then evaluated for all nodes N in the grid, which results in the following global sparse block linear system:

$$\begin{bmatrix} C_{1,dx} & C_{1,dy} \\ C_{2,dx} & C_{2,dy} \end{bmatrix} \begin{bmatrix} \frac{\partial \phi}{\partial x}(\mathbf{x_1}) \\ \vdots \\ \frac{\partial \phi}{\partial x}(\mathbf{x_N}) \\ \frac{\partial \phi}{\partial y}(\mathbf{x_1}) \\ \vdots \\ \frac{\partial \phi}{\partial y}(\mathbf{x_N}) \end{bmatrix} = \begin{bmatrix} C_{1,x} & 0 \\ 0 & C_{2,dy} \end{bmatrix} \begin{bmatrix} \phi(\mathbf{x_1}) \\ \vdots \\ \phi(\mathbf{x_N}) \\ \phi(\mathbf{x_1}) \\ \vdots \\ \phi(\mathbf{x_N}) \end{bmatrix} \tag{13}$$

expressed as

$$P_{2D} \begin{bmatrix} \frac{\partial \boldsymbol{\phi}}{\partial x} \\ \frac{\partial \boldsymbol{\phi}}{\partial y} \end{bmatrix} = Q_{2D} \begin{bmatrix} \boldsymbol{\phi} \\ \boldsymbol{\phi} \end{bmatrix} \tag{14}$$

The order of the solution of Eq. (14), depend on the polynomial order K in Eq. (3). In the current formulation, the order of the scheme is increased by including connectivity from neighbouring gradients, allowing a higher polynomial order K in Eq. (3) while maintaining the compact formulation of only including neighbours according to the stencil in Fig. 1. The effective stencil however, incurred in Eq, (13), then span over the entire grid. This method will be referred to implicit LSQ (ILSQ).

The coefficients of P_{2D} and Q_{2D} only depend on grid metrics, if the grid is stationary these can be computed in preprocessing step. The appearance of the off-diagonal block elements $C_{1,dy}, C_{2,dx}$ in Eq. (13) is a result due to the formulation of the two-dimensional polynomial expansion in Eq. (3) and the solution of the least square system in Eq. (10). For a uniform cartesian grid, the resulting coefficients in $C_{1,dy}$ and $C_{2,dx}$ are zero. The coefficients in P_{2D} and Q_{2D} then reduce to the 1D case in Eq. (1) in each coordinate direction, with coefficients according to the classical compact fourth-order formula [9, 10]

$$\frac{1}{4}\left(\frac{\partial \phi}{\partial x}\right)_{i+1} + \left(\frac{\partial \phi}{\partial x}\right)_i + \frac{1}{4}\left(\frac{\partial \phi}{\partial x}\right)_{i-1} = \frac{3}{4}\frac{\phi_{i+1} - \phi_{i-1}}{\Delta x} \tag{15}$$

A. Boundary Conditions

In this paper, the high-order compact gradient scheme is only considered for interior nodes. For a Neumann boundary condition, the gradients are specified at the boundary and the coefficients in Eq. (14) may be moved to the right hand side. For a Dirichlet boundary condition, the boundary nodes requires special care. According to Gustafsson [20], the global order of the scheme is conserved if the boundary nodes are closed with one order less than the interior nodes. For the ILSQ scheme with target fourth-order accuracy, the boundaries need to be closed with at least third-order accuracy. Methods of deriving appropriate high-order boundary schemes are e.g. based on one-sided formulas [9, 10, 21] or the so-called Summation-By-Parts [22] which can be also applied for high-order compact gradients schemes.

B. Solution of Linear System

The size of the matrices P_{2D} and Q_{2D} in Eq. (14) are $4N^2$, the corresponding system in 3D have size $9N^2$. As the compact discretisation leads to a non-symmetric matrix P_{2D} for unstructured grids, Eq. (14) is solved with ILU preconditioned biconjugate gradient stabilized method (BiCGStab) [23]. In the test cases considered in Section IV, the BiCGStab solver requires only a couple of iterations to reach the set tolerance of 10^{-8} of the linear solver. If there is enough memory space available the solution of Eq. (14), $P_{2D}^{-1}Q_{2D}$, may be precomputed and stored in a preprocessing step.

III. Explicit Gradient Reconstruction

The implicit gradient scheme is compared to an explicit LSQ (ELSQ), which for a second-order polynomial can be formulated as

$$\begin{bmatrix} w_{i1}\Delta x_{i1} & w_{i1}\Delta y_{i1} & w_{i1}\Delta x_{i1}^2 & w_{i1}\Delta x_{i1}\Delta y_{i1} & w_{i1}\Delta y_{i1}^2 \\ \vdots & \vdots & \vdots & \vdots & \vdots \\ w_{ij}\Delta x_{ij} & w_{ij}\Delta y_{ij} & w_{ij}\Delta x_{ij}^2 & w_{ij}\Delta x_{ij}\Delta y_{ij} & w_{ij}\Delta y_{ij}^2 \\ \vdots & \vdots & \vdots & \vdots & \vdots \\ w_{iN_b}\Delta x_{iN_b} & w_{iN_b}\Delta y_{iN_b} & w_{iN_b}\Delta x_{iN_b}^2 & w_{iN_b}\Delta x_{iN_b}\Delta y_{iN_b} & w_{iN_b}\Delta y_{iN_b}^2 \end{bmatrix} \begin{bmatrix} L_{i,x}\frac{\partial \phi}{\partial x}(\mathbf{x_i}) \\ L_{i,y}\frac{\partial \phi}{\partial y}(\mathbf{x_i}) \\ \vdots \end{bmatrix} = \begin{bmatrix} w_{i1}(\phi_i(\mathbf{x_i}) - \phi(\mathbf{x_1})) \\ \vdots \\ w_{ij}(\phi_i(\mathbf{x_i}) - \phi(\mathbf{x_j})) \\ \vdots \\ w_{iN_b}(\phi_i(\mathbf{x_i}) - \phi(\mathbf{x_{N_b}})) \end{bmatrix} \tag{16}$$

where $\Delta x_{ij}, \Delta y_{ij}$ are given in Eq. (4). The explicit least-squares problem in Eq. (16) is solved using QR-decomposition according to Eq. (10). We investigate two different variants of Eq. (16). The first one is according to the standard distance weighted LSQ [24–26] (WLSQ) scheme, where the following weights and normalization factors are chosen as:

$$w_{ij} = \frac{1}{d_{ij}},\ L_{i,x} = 1,\ L_{i,y} = 1 \tag{17}$$

where d_{ij} is defined in Eq. (6). It is shown in Section IV that the order and accuracy of this formulation deteriorates on grids with high-aspect-ratio. In order to alleviate this problem, we propose a similar but different variant by choosing the following weights and normalization factors:

$$w_{ij} = 1,\ L_{i,x},\ L_{i,y} \tag{18}$$

where $L_{i,x},\ L_{i,y}$ can be either of the normalization methods defined by Eqs. (5), (7) or (8). This method will be referred to as modified LSQ (MLSQ). By choosing normalization method according to Eq. (7) or (8), the local grid spacing in each coordinate direction is used instead of the maximum length method given by Eq. (5), which should intuitively be more valid in regions with high-aspect-ratio elements. In order to increase the order and accuracy of an ELSQ gradient reconstruction scheme, one can increase the amount of node candidates by including neighbours to nearest neighbours. However, the compact formulation is then lost and the implementations on an unstructured grid may become increasingly complicated.

IV. Analysis and Assessment of Gradient Reconstruction

In order to assess the order, accuracy and robustness of the gradient reconstruction schemes, the numerical gradient of a known smooth test function is compared to its analytical value on consecutively refined meshes [6, 8]. The function is evaluated for each interior node repeatedly through several refinement levels for a set of different structured,

unstructured, isotropic and high-aspect-ratio grids. The L_1 and L_2 errors in the resulting numerical gradient are calculated as

$$L_1 = \frac{\sum_i^N |\nabla\phi_{i,num} - \nabla\phi_{i,ana}|}{N}, \quad L_2 = \left(\frac{\sum_i^N |\nabla\phi_{i,num} - \nabla\phi_{i,ana}|^2}{N} \right)^{1/2}, \tag{19}$$

where $\nabla\phi_{i,num}$ and $\nabla\phi_{i,ana}$ are the numerical and analytical gradients, respectively. The implicit (ILSQ) scheme is evaluated for a polynomial order $K = 4$ in Eq. (3) using the normalization given by Eq. (8), unless otherwise stated. We set the tolerance of the BiCGStab solver to 10^{-8} measured in the L_2 norm of the residual. Since the accuracy of interior nodes of in the scope of this work, it is assumed that the gradient values at the boundary are known. The compact implicit gradient scheme is compared to the standard distance weighted explicit LSQ (WLSQ) gradient reconstruction scheme (Eq. (16)), with weighting and normalization factors according to Eq. (17). The modified LSQ (MLSQ) scheme is also considered, with weighting and normalization factors according to Eq. (18). We consider only neighbours included in the LSQ formulation according to Fig. 1. This limits the ELSQ schemes to maximum second-order schemes.

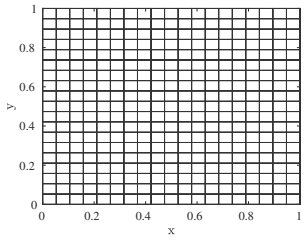

(a) Uniform quadrilaterals.

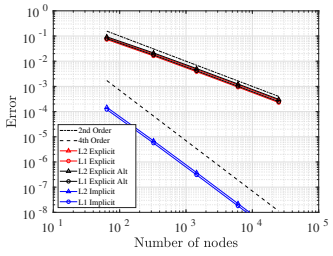

(b) Error on grid Fig. 2(a).

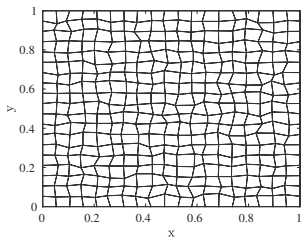

(c) Perturbed quadrilaterals.

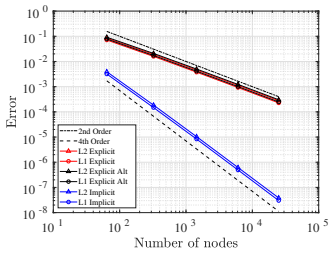

(d) Error on grid Fig. 2(c).

Fig. 2 Error convergence of gradient reconstruction of the function given by Eq. (20)**, using WLSQ (red), MLSQ (black) and ILSQ (blue) gradients on isotropic quadrilateral grids.**

A. Isotropic Grids

The test function is given by:

$$f(x, y) = \sin(\pi x) \sin(\pi y) \tag{20}$$

Function (20) is evaluated on a rectangular domain given by $[0, 1] \times [0, 1]$, discretized with quadrilaterals or mixed elements (quadrilaterals and triangles).

Results on the isotropic quadrilateral set of grids are shown in Fig. 2. Error convergence results for the interior nodes are given in Figs. 2(b) and 2(d). The ILSQ scheme yields fourth-order accuracy on both the uniform and the perturbed quadrilateral grids. The vertices of the grid in Fig. 2(c) are randomly disturbed compared to the grid Fig. 2(a), and as a result, the underlying structure is lost. This produces a one order of magnitude larger error level for the ILSQ scheme, however, the fourth-order scaling is still preserved. The two different ELSQ schemes show the expected second-order accuracy on both grids, where the two different formulations show a negligible difference in error.

We consider uniform and perturbed mixed element grids for the same function. The two different grids are shown in Figs. 3(a) and 3(c). The grids are generated from a quadrilateral grid, where for each element, there is a 50 % probability that the quadrilateral element will be split into two triangles. The error convergence are given in Figs. 3(b) and 3(d).

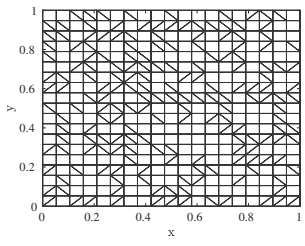

(a) Uniform mixed elements.

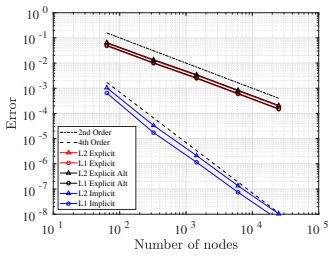

(b) Error on grid Fig. 3(a).

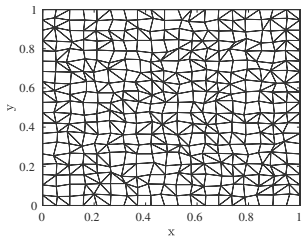

(c) Perturbed mixed elements.

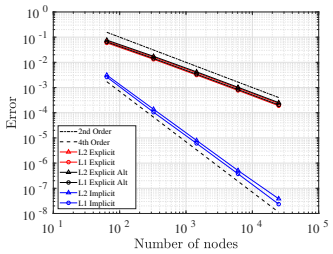

(d) Error on grid Fig. 3(c).

Fig. 3 Error convergence of gradient reconstruction of the function given by Eq. (20)**, using WLSQ (red), MLSQ (black) and ILSQ (blue) gradients on isotropic mixed element grids.**

All methods yield the prescribed accuracy, the ILSQ shows fourth-order convergence and the two different ELSQ schemes show second-order convergence, on both the uniform and perturbed grids. The error levels are comparable to the quadrilateral grids considered in Fig. 2, which indicates that the LSQ gradient reconstruction formulation is insensitive to grids with mixed quadrilaterals and triangles.

B. High-aspect-ratio-grids

The test function is given by:

$$f(x, y) = \sin(\pi x)\sin(4000\pi y) \tag{21}$$

Equation (21) is evaluated on a rectangular domain given by $[0, 1] \times [0, 0.0005]$. Using this domain size, elements with aspect-ratio of 2000 is considered. This setup models a typical boundary layer problem [8], where the solution variation is predominant in the direction of small grid spacing and an anisotropic grid is specifically tailored to represent the solution anisotropy. Five types of grids are considered: uniform quadrilateral, perturbed quadrilateral, uniform mixed elements, perturbed mixed elements and perturbed fully triangular grids.

The quadrilateral grids are shown in Figs. 4(a) and 4(c), error convergence results on these grids are shown in Figs. 4(b) and 4(d). The error convergence results are similar to the isotropic quadrilateral grids, the ISLQ scheme yields fourth-order accuracy, the two ELSQ schemes yield second-order accuracy. However, on the perturbed quadrilateral grid, the WLSQ method breaks down and even yields larger errors with increased grid refinement. On the same grid, the ILSQ and MLSQ methods yield the prescribed accuracy, fourth-order for ILSQ and second-order for MLSQ.

Results for the mixed element grids are shown in Figs. 5(a). and 5(c), error convergence results on these grids are shown in Figs. 5(b) and 5(d). The error convergence results are similar to the isotropic mixed element grids, the ISLQ scheme yields fourth-order accuracy, the two ELSQ schemes yield second-order accuracy. Similar to the high-aspect-ratio uniform quadrilateral grid, the WLSQ method fails to recover second-order on the perturbed mixed element grids, as can be seen in Fig. 5(d). On the same grid, the ILSQ and MLSQ methods yield the prescribed

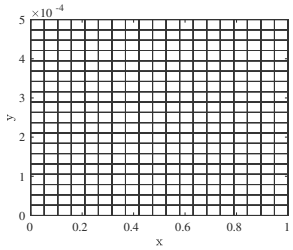

(a) Uniform quadrilaterals.

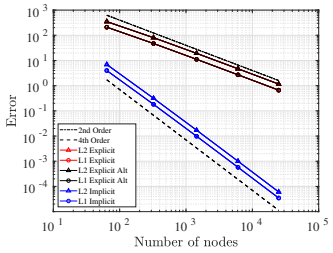

(b) Error on grid Fig. 4(a).

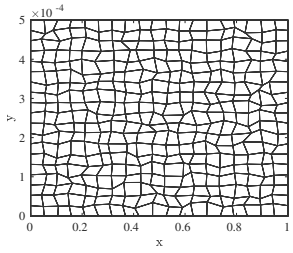

(c) Perturbed quadrilaterals.

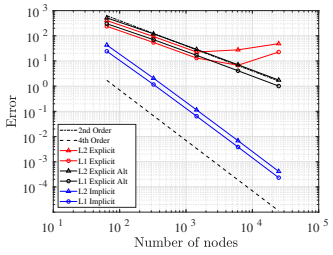

(d) Error on grid Fig. 4(c).

Fig. 4 Error convergence of gradient reconstruction of the function given by Eq. (21)**, using WLSQ (red), MLSQ (black) and ILSQ (blue) gradients on high-aspect-ratio quadrilateral grids.**

accuracy, fourth-order for ILSQ and second-order for MLSQ. Remarkably, the accuracy is preserved for the ILSQ and MLSQ although these grids are irregular and involve two different types of cell stencils.

Finally, the effects of using different normalization given by Eqs. (5), (7), (8) are investigated for the ILSQ and the MLSQ. A perturbed triangular grid is considered (Fig. 6). Results for the error convergence are shown in Figs. 6(b), 6(c) and 6(d). Similar to WLSQ, the ILSQ using the length based normalization according to Eq. (5) completely fails to reconstruct the gradients. However, this is not observed for the MLSQ using the same normalization method. This can be attributed to that the MLSQ only assumes a second-order polynomial, whereas the ILSQ assumes a fourth-order polynomial, which should be more sensitive to specific choice of normalization. The ILSQ is able to recover the fourth-order accuracy by using the normalization according to Eqs. (8) or (7). These methods take the local grid spacing in each direction into account and is thus more accurate and robust compared to the length based approach given by Eq. (5) on grids with high-aspect-ratio.

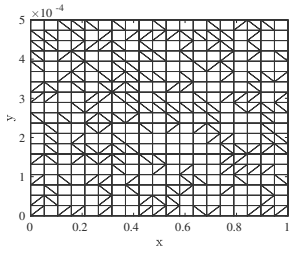

(a) Mixed elements.

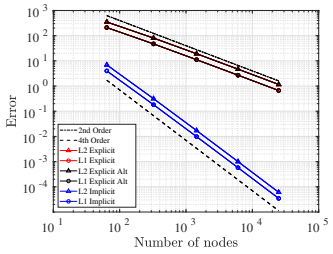

(b) Error on grid Fig. 5(a).

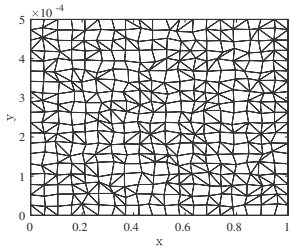

(c) Uniform quadrilaterals.

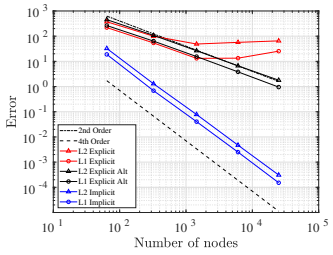

(d) Error on grid Fig. 5(c).

Fig. 5 Error convergence of gradient reconstruction of the function given by Eq. (21)**, using WLSQ (red), MLSQ (black) and ILSQ (blue) gradients on high-aspect-ratio mixed elements grids.**

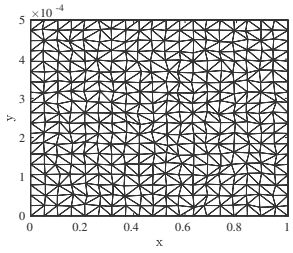

(a) Perturbed triangles.

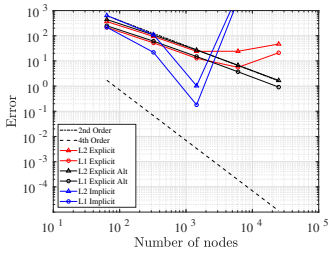

(b) Normalization given by Eq. (5).

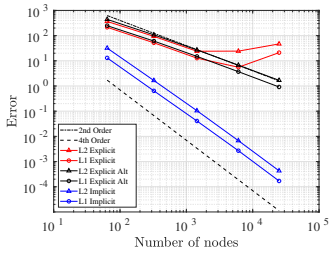

(c) Normalization given by Eq. (8).

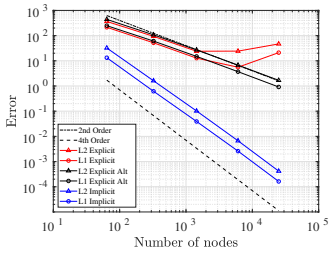

(d) Normalization given by Eq. (7).

Fig. 6 Error convergence of gradient reconstruction of the function given by Eq. (21)**, using WLSQ (red), MLSQ (black) and ILSQ (blue) gradients on high-aspect-ratio triangular grids. Effects of using different normalizations given by Eqs.** (5)**,** (7) **or** (8)**.**

V. Conclusions and future work

An implicit least squares gradient reconstruction scheme with a compact formulation is derived and compared with a standard distance weighted explicit least squares scheme. Additionally, a modified explicit least squares scheme is formulated, which uses different weighting compared to the standard method. The schemes only use neighbouring nodal values and can be viewed as unstructured finite difference schemes. A detailed study of gradient calculation for node-centered unstructured data on regular, highly irregular and high-aspect-ratio ($AR = 2000$) grids is presented.

Compared to a standard distance weighted LSQ scheme, which uses only nodal values of nearest neighbours in the stencil, the implicit scheme also includes information from neighbouring gradient values, leading to a linear system to be solved. This allows the assumed polynomial or Taylor expansion in the least squares approach to be of higher order. In this study, a fourth-order polynomial is assumed for the implicit LSQ scheme, and a second-order polynomial is assumed for the explicit LSQ schemes.

The schemes are assessed in the capability of reconstructing the gradient of a known analytical function. The implicit LSQ shows a fourth-order scaling on all grids considered, including highly irregular quadrilateral grids, triangular grids, mixed element grids and high-aspect-ratio grids. The standard distance weighted LSQ scheme, on the other hand, fails to achieve the prescribed second-order accuracy on high-aspect-ratio grids, where even the error is increased with grid refinement. The modified explicit least squares scheme, which uses the local grid spacing in each coordinate direction in the weighting procedure, is able to achieve second-order accuracy on high-aspect-ratio grids.

The current study is planned to be followed up by an implementation of the new scheme in an unstructured compressible finite-volume flow solver, where the accuracy, feasibility and robustness will be investigated on relevant flow cases.

Acknowledgement

This work has been funded by the Swedish Governmental Agency for Innovation Systems (VINNOVA), the Swedish Defence Materiel Administration (FMV) and the Swedish Armed Forces within the National Aviation Research Programme (NFFP, Contract No. 2017–04887) and Saab Aeronautics.

References

[1] Diskin, B., T., J. L., Nielsen, E. J., Nishikawa, H., and White, J. A., "Comparison of Node-Centered and Cell-Centered Unstructured Finite-Volume Discretizations: Viscous Fluxes," *AIAA Journal*, Vol. 48, No. 7, 2010, pp. 1326–1338. https://doi.org/10.2514/1.44940.

[2] Diskin, B., and T., J. L., "Comparison of Node-Centered and Cell-Centered Unstructured Finite-Volume Discretizations: Inviscid Fluxes," *AIAA Journal*, Vol. 49, No. 4, 2011, pp. 836–854. https://doi.org/10.2514/1.J050897.

[3] Eliasson, P., "Edge, a Navier–Stokes solver for unstructured grids," *Finite Volumes for Complex Applications*, CP849, Vol. III, 2002, pp. 527–534.

[4] Eliasson, P., and Weinerfelt, P., "Recent applications of the flow solver Edge," *7th Asian CFD Conference*, 2007.

[5] Moukalled, F., Mangani, L., and Darwish, M., *The Finite Volume Method in Computational Fluid Dynamics: An Advanced Introduction with OpenFOAM and Matlab*, 1st ed., Springer Publishing Company, Incorporated, 2015.

[6] Ollivier-Gooch, C., Nejat, A., and M., K., "Obtaining and Verifying High-Order Unstructured Finite Volume Solutions to the Euler Equations," *AIAA Journal*, Vol. 47, No. 9, 2009, pp. 2105–2120. https://doi.org/10.2514/1.40585.

[7] Wang, Q., Ren, Y.-X., Pan, J., and Li, W., "Compact high order finite volume method on unstructured grids III: Variational reconstruction," *Journal of Computational Physics*, Vol. 337, 2017, pp. 1–26. https://doi.org/https://doi.org/10.1016/j.jcp.2017.02.031.

[8] Nishikawa, H., "From hyperbolic diffusion scheme to gradient method: Implicit Green–Gauss gradients for unstructured grids," *Journal of Computational Physics*, Vol. 372, 2018, pp. 126–160. https://doi.org/https://doi.org/10.1016/j.jcp.2018.06.019.

[9] Lele, S. K., "Compact finite difference schemes with spectral-like resolution," *Journal of Computational Physics*, Vol. 103, No. 1, 1992, pp. 16–42. https://doi.org/https://doi.org/10.1016/0021-9991(92)90324-R.

[10] Carpenter, M. H., Gottlieb, D., and Abarbanel, S., "Stable and accurate boundary treatments for compact, high-order finite-difference schemes," *Applied Numerical Mathematics*, Vol. 12, No. 1, 1993, pp. 55–87. https://doi.org/https://doi.org/10.1016/0168-9274(93)90112-5, sPECIAL ISSUE.

[11] Visbal, M. R., and Gaitonde, D. V., "High-Order-Accurate Methods for Complex Unsteady Subsonic Flows," *AIAA Journal*, Vol. 37, No. 10, 1999, pp. 1231–1239. https://doi.org/10.2514/2.591.

[12] Shukla, R. K., and Zhong, X., "Derivation of high-order compact finite difference schemes for non-uniform grid using polynomial interpolation," *Journal of Computational Physics*, Vol. 204, No. 2, 2005, pp. 404–429. https://doi.org/https://doi.org/10.1016/j.jcp.2004.10.014.

[13] Shukla, R. K., Tatineni, M., and Zhong, X., "Very high-order compact finite difference schemes on non-uniform grids for incompressible Navier–Stokes equations," *Journal of Computational Physics*, Vol. 224, No. 2, 2007, pp. 1064–1094. https://doi.org/https://doi.org/10.1016/j.jcp.2006.11.007.

[14] Pandit, S. K., Kalita, J. C., and Dalal, D., "A transient higher order compact scheme for incompressible viscous flows on geometries beyond rectangular," *Journal of Computational Physics*, Vol. 225, No. 1, 2007, pp. 1100–1124. https://doi.org/https://doi.org/10.1016/j.jcp.2007.01.016.

[15] Pandit, S. K., and Chattopadhyay, A., "A robust higher order compact scheme for solving general second order partial differential equation with derivative source terms on nonuniform curvilinear meshes," *Computers Mathematics with Applications*, Vol. 74, No. 6, 2017, pp. 1414–1434. https://doi.org/https://doi.org/10.1016/j.camwa.2017.06.031.

[16] Fishelov, D., "A new fourth-order compact scheme for the Navier–Stokes equations in irregular domains," *Computers Mathematics with Applications*, Vol. 74, No. 1, 2017, pp. 6–25. https://doi.org/https://doi.org/10.1016/j.camwa.2016.10.020, 5th European Seminar on Computing ESCO 2016.

[17] Ferziger, J. H., and P., M., *Computational Methods for Fluid Dynamics*, 2nd ed., Springer, Berlin, 1999.

[18] Luo, H., Baum, J. D., and Löhner, R., "A discontinuous Galerkin method based on a Taylor basis for the compressible flows on arbitrary grids," *Journal of Computational Physics*, Vol. 227, No. 20, 2008, pp. 8875–8893. https://doi.org/https://doi.org/10.1016/j.jcp.2008.06.035.

[19] Strang, G., *Linear Algebra and its Application*, 2nd ed., Academic Press, 1980. https://doi.org/https://doi.org/10.1016/B978-0-12-673660-1.50003-4.

[20] Gustafsson, B., "The Convergence Rate for Difference Approximations to Mixed Initial Boundary Value Problems," *Mathematics of Computation*, Vol. 29, No. 130, 1975, pp. 396–406.

[21] Svärd, M., and Nordström, J., "On the order of accuracy for difference approximations of initial-boundary value problems," *Journal of Computational Physics*, Vol. 218, No. 1, 2006, pp. 333–352. https://doi.org/https://doi.org/10.1016/j.jcp.2006.02.014.

[22] Svärd, M., and Nordström, J., "Review of summation-by-parts schemes for initial–boundary-value problems," *Journal of Computational Physics*, Vol. 268, 2014, pp. 17–38. https://doi.org/https://doi.org/10.1016/j.jcp.2014.02.031.

[23] van der Vorst, H. A., "Bi-CGSTAB: A Fast and Smoothly Converging Variant of Bi-CG for the Solution of Nonsymmetric Linear Systems," *SIAM Journal on Scientific and Statistical Computing*, Vol. 13, No. 2, 1992, pp. 631–644. https://doi.org/10.1137/0913035.

[24] Mavriplis, D., *Revisiting the Least-Squares Procedure for Gradient Reconstruction on Unstructured Meshes*, ???? https://doi.org/10.2514/6.2003-3986.

[25] Zhang, F., "A vertex-weighted-Least-Squares gradient reconstruction," , 2017. https://doi.org/10.48550/ARXIV.1702.04518.

[26] Nishikawa, H., and White, J. A., "An efficient cell-centered finite-volume method with face-averaged nodal-gradients for triangular grids," *Journal of Computational Physics*, Vol. 411, 2020, p. 109423. https://doi.org/https://doi.org/10.1016/j.jcp.2020.109423.